

# Wavenumber Domain Focusing of Squinted SAR Data with a Curved Orbit Geometry.

Thierry Michel and Scott Hensley  
 Jet Propulsion Laboratory, California Institute of Technology  
 4800 Oak Grove Drive, Pasadena, CA 91109, USA

*Email:* Thierry.Michel@jpl.nasa.gov

**Abstract**—Synthetic Aperture Radar systems provide raw data that need focusing to achieve full-resolution imaging. Current SAR applications, including interferometry, require accurate, phase-preserving, and precisely co-registered coherent images over large ground swaths with the highest achievable resolution. In addition to these challenges, stripmap SAR data may be acquired with an off-broadside (squinted) geometry, either by design or through platform motion. The precise batch focusing of these large aperture and wide bandwidth data sets is known to require a 2D frequency processing approach. The standard wave domain focusing algorithm, however, is only exact for data acquired on a rectilinear trajectory. We investigate a generalization of the standard omega-k focusing formulation that allows curved data acquisition tracks. The new formulation can be used in conjunction with a known extension for conical, squinted imaging grids. The approximations necessary to allow the generalized geometry are analysed to determine the range of applicability of the proposed algorithm. The theory is validated using data simulated with parameters similar to the UAVSAR L-band SAR system.

## I. INTRODUCTION

SAR systems using wide bandwidths and low frequencies are being developed for new sensors and applications that require a high azimuth resolution. The approximation made in traditional SAR processing algorithms that range migration and azimuth focusing are strictly one-dimensional operations in range-Doppler coordinates is invalid for these new radar configurations. Wave domain migration algorithms are known to provide optimal focusing in such cases [4][5][1][12][11][10]. However, these algorithms assume a rectilinear flight path, while the actual sensor might follow a curved track, or orbit. A motion compensation procedure is then required to correct deviations from a straight line due to the earth's curvature. Wide azimuth beamwidth and large bandwidth systems yield motion compensation displacements which depend on the instantaneous position of the target within the antenna beam and can be difficult to compensate. A focusing operator modified to correct for curved antenna tracks minimizes the need for, or the extent of motion compensation as a requirement for accurate processing. In earlier work,

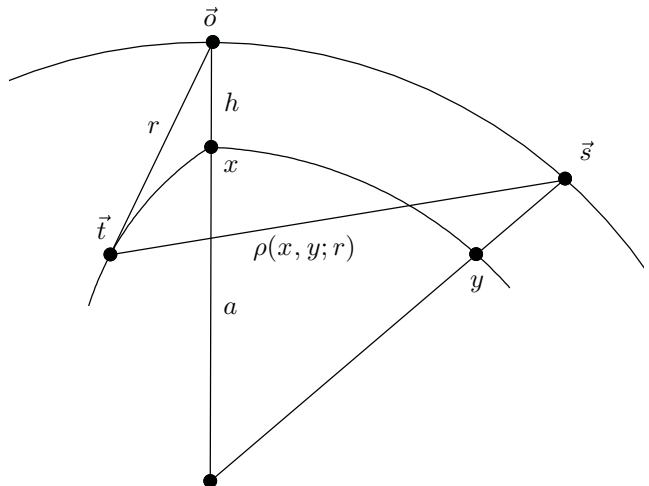


**Figure 1.** Antenna track and image reference geometry: antenna  $\vec{s}$  and scatterer  $\vec{t}$ ;  $\vec{ot} \perp \vec{os}$  for  $y \rightarrow x$ .  $a$  is the radius of the earth.  $h$  the platform altitude.

the aperture curvature problems was addressed through motion compensation [9], through the introduction of an effective platform velocity [3], or also through a Singular Value Decomposition (SVD) of the wavenumber domain propagation phase [6][7]. In this work, an exact expression for the phase history is exploited to justify a simple factorization of the migration phase that provides high focusing accuracy for air- or spaceborne systems.

## II. FOCUSING FROM STATIONARY PHASE PRINCIPLE

A model for a fully focused and geometrically correct SAR image  $S(x, r)$  produced from the acquired RF data  $D(x, \tau)$  is obtained by filtering the raw data by the space-variant system impulse response:

$$S(x, r) = \iint dy d\tau \frac{w(x-y)}{\rho^P} D(y, \tau) h[\rho(x, y; r) - \tau]. \quad (1)$$

The raw data  $D$ , coherent image  $S$ , and transmitted waveform  $h$  are RF modulated signals, before down-conversion and filtering. The range propagation offset  $\tau$  of  $D(x, \tau)$  and  $h(\tau)$  is the length  $\tau = (2/c) * t$ , where time  $t$  is the two-way echo delay and  $c$ , the speed of light. Coordinates  $x$  and  $y$  are along track arc lengths,  $\|\vec{ot}\| = r$  is

the broadside slant range in a plane perpendicular to the orbit plane,  $\|\vec{s}\vec{t}\| = \rho(x, y; r)$  is the slant range history from antenna  $\vec{s}$  at  $y$  to image point  $\vec{t}(x, r)$ . Factors  $w$  and  $\rho^{-P}$  compensate the radiometric antenna and range weighting, and will be discarded for convenience:  $w = 1$ ,  $P = 0$ . Performing the range convolution of Eq.[1] in the Fourier domain and assuming that range compression has been carried out,  $\bar{h}(k_\omega) = 1$ , focusing is seen to consist of the removal of a pure phase propagation factor:

$$S(x, r) = \int dy \int dk_\omega \bar{D}(y, k_\omega) e^{ik_\omega \rho(x, y; r)}, \quad (2)$$

in which the notation  $\bar{D}$  and  $\bar{h}$  means that a  $[\tau \rightarrow k_\omega]$  Fourier transform on  $D$  or  $h$  has been carried out. Note that  $D$  and  $S$  have implicit carriers, while  $S^{\omega_0}$  and  $D^{\omega_0}$  are basebanded and band-limited:

$$D(x, \tau) = D^{\omega_0}(x, \tau) e^{ik_{\omega_0} \tau}, \quad S(x, r) = S^{k_{r_0}}(x, \tau) e^{ik_{r_0} \tau}.$$

Assuming that the slant-range history is stationary  $\rho(x, y; r) = \rho(x - y, r)$ , the range variant along track convolution becomes the product of the data with a phase transfer function  $I$  in the 2D wave domain  $[\tau \rightarrow k_\omega, x \rightarrow k_x]$ :

$$\begin{aligned} \bar{S}(k_x, r) &= \int dk_\omega \bar{D}(k_x, k_\omega) I(k_x, k_\omega; r) \\ I(k_x, k_\omega; r) &= \int dx e^{ik_\omega \varphi(x, r; k_x/k_\omega)}, \\ \varphi(x, r; k_x/k_\omega) &= \rho(x, r) - \frac{k_x x}{k_\omega}. \end{aligned} \quad (3)$$

The wavenumber domain focusing phase factor  $I(k_x, k_\omega; r)$  can be simplified in this geometry using the principle of stationary phase (SP.) The antenna track is assumed to produce range histories with along track derivatives varying slowly enough to be able to assume uniqueness of the SP point  $\tilde{x}$  at which the phase derivative  $\partial\varphi/\partial x = \partial\rho/\partial x - k_x/k_\omega$  vanishes. A reasonably stable platforms satisfy this requirement. The SP point  $\tilde{x}$  is the point where the dimensionless Doppler angle  $y = k_x/k_\omega$  equals the slant range along track slope  $\partial\rho(x, r)/\partial x$ , or  $\rho'_x(\tilde{x}, r) = y$ , in the domain  $|y| \leq 1$ . The SP phase  $\varphi(\tilde{x}(y), r; y) = \phi(y, r)$  can be evaluated two ways: ,

- 1:  $\phi(y, r) = \rho(\tilde{x}(y, r), r) - y\tilde{x}(y, r)$ , or
- 2:  $\phi'_y(y, r) = -\tilde{x}(y, r) \longrightarrow \phi(y, r) = -\int^y dy' \tilde{x}(y', r)$ .

Once the stationary phase is known, the wavenumber domain transfer function is a range and frequency dependent phase factor that is applied to the 2D transform of the data:

$$\bar{S}(k_x, r) = \int dk_\omega \bar{D}(k_x, k_\omega) e^{ik_\omega \phi(k_x/k_\omega, r)}. \quad (4)$$

Slowly varying amplitude factors are ignored for clarity.

### III. STRAIGHT AND CURVED APERTURES

Next we apply the above approach to two types of antenna trajectories. In the well-known linear case,

$$\begin{cases} \rho(x, r) = \sqrt{r^2 + x^2}, & \rho'_x(x, r) = \frac{x}{\sqrt{r^2 + x^2}}, \\ \rho'_x(\tilde{x}, r) = y, & \tilde{x}(y, r) = r \frac{y}{\sqrt{1 - y^2}}, \\ \phi(y, r) = r\sqrt{1 - y^2}, & \phi'_y(y, r) = -\tilde{x}(y, r), \end{cases}$$

the SP phase has the separable form  $\phi(y, r) = r\sqrt{1 - y^2}$ . With the wavenumber definition  $k_r = \sqrt{k_\omega^2 - k_x^2}$ , Eq. [4] becomes a Fourier transform:

$$\begin{aligned} \bar{S}(k_x, r) &= \int dk_\omega \bar{D}(k_x, k_\omega) e^{ik_r r}, \\ \bar{S}(k_x, k_r) &= \bar{D}(k_x, k_\omega). \end{aligned} \quad (5)$$

Equation [5] is the familiar results that the band-limited transform of the object is the transform of the data.

In the case where the trajectory is a circular arc, which is a good approximation for orbit segments within the synthetic aperture, taking  $a$  as the local earth radius,  $h$  as the platform altitude, and  $x$  and  $y$  as arc lengths with radius  $a$  (see Figure [2]), the slant range history and slope are:

$$\begin{aligned} \rho(x, r) &= \sqrt{r^2 + 2\gamma(r) \sin^2\left(\frac{x}{2a}\right)}, \\ \gamma(r) &= (h + a)^2 + a^2 - r^2, \\ \rho'_x(x, r) &= \frac{\gamma(r) \sin\left(\frac{x}{a}\right)}{2a\sqrt{r^2 + 2\gamma(r) \sin^2\left(\frac{x}{2a}\right)}}. \end{aligned}$$

The reference range  $r$  is taken as the distance of closest approach, in the plane perpendicular to the plane of the arc. The SP point  $\tilde{x}$  is obtained from  $\rho'_x(\tilde{x}, r) = y$  with solutions:

$$\tilde{x}(y, r) = \pm 2a \arcsin \sqrt{b(1 - \sqrt{1 - c/b^2})}, \quad \begin{cases} b = \frac{1}{2} - \frac{a^2 y^2}{\gamma(r)} \\ c = \left(\frac{ayr}{\gamma(r)}\right)^2. \end{cases}$$

A quartic equation in the slant range  $\rho$  relating it to the range slope  $y = \partial\rho/\partial x$ , the reference range  $r$ , and the sphere radius  $a$  and orbit height  $h$ , can also be exploited to solve for  $\rho(\tilde{x}(y), r)$ :

$$\rho^4 + (4y^2 a^2 - 2r^2 - 2\gamma(r)) \rho^2 + r^4 + 2\gamma(r) r^2 = 0.$$

There are again two ways to the compute the SP :

$$\phi(y, r) = \rho(\tilde{x}(y, r), r) - y\tilde{x}(y, r) = -\int^y dy' \tilde{x}(y', r).$$

However, unlike in the linear case, the migration phase of Eq.[4] for a curved aperture is not separable into a range factor  $R$  and frequency factor  $Q$  :

$$\phi(y, r) \neq Q(y)R(r),$$

which prevents mapping the Fourier data domain into the image domain as in the linear case Eq.[5].

#### IV. RANGE-FREQUENCY MIGRATION SEPARABILITY

A series expansion of the stationary phase in powers of  $h/a$  is used to estimate the errors of separable approximations to the phase  $\phi(y, r)$ . This expansion bridges the gap between the separable linear case and the curved case ( $h/a = 0$ ):

$$\phi(y, r) \underset{a \rightarrow \infty}{\cong} r \left[ \sqrt{1-y^2} + \frac{h}{2a} \frac{y^2}{\sqrt{1-y^2}} + \frac{h^2}{8a^2} \frac{y^2(y^2-2)}{(1-y^2)^{3/2}} + \frac{r^2}{24a^2} \frac{y^2(5y^2-6)}{(1-y^2)^{3/2}} + O\left(\frac{h^3}{a^3}\right) \right]. \quad (6)$$

The lowest order term is exactly the expression found in the linear case:  $k_\omega \phi^{(0)}(k_x/k_\omega, r) = k_r r$ . The first order term is separable (linear in  $r$ ) and quadratic in  $k_x$  :

$$k_\omega \phi^{(1)}\left(\frac{k_x}{k_\omega}, r\right) = \frac{h}{2a} \frac{k_x^2}{k_r} r. \quad (7)$$

This term compensates a change in range curvature due to the deviation of the circular orbit from a straight line. The second order terms  $(h/a)^2$  has two contributions, one is cubic in  $r$  and is the lowest order unseparable term :

$$k_\omega \phi^{(2)}\left(\frac{k_x}{k_\omega}, r\right) = \frac{h^2}{8a^2} \frac{k_x^2(k_x^2 - 2k_\omega^2)}{k_r^3} r + \frac{r^2}{24a^2} \frac{k_x^2(5k_x^2 - 6k_\omega^2)}{k_r^3} r.$$

The magnitude of that term determines the range of validity of a separable approximation to the migration phase. Since only the range dependent part of that term is non-separable, its range factor  $r^2$  may be fixed mid-swath  $r^2 \rightarrow r_{\text{mid}}^2$ . Up to second order in  $h/a$ , the separable phase model becomes:

$$\phi\left(\frac{k_x}{k_\omega}, r\right) \cong Q_a\left(\frac{k_x}{k_\omega}\right) R_a(r), \quad R_a(r) = r, \quad (8)$$

$$k_\omega Q_a\left(\frac{k_x}{k_\omega}\right) = k_r + \frac{h}{2a} \frac{k_x^2}{k_r} + \frac{h^2}{8a^2} \frac{k_x^2(k_x^2 - 2k_\omega^2)}{k_r^3} + \frac{r_{\text{mid}}^2}{24a^2} \frac{k_x^2(5k_x^2 - 6k_\omega^2)}{k_r^3}.$$

The purpose of the series expansion is to provide a phase error estimates  $k_\omega \delta \phi$  for the  $QR$  separation of Eq.[8]:

$$k_\omega \delta \phi\left(\frac{k_x}{k_\omega}\right) = (r_{\text{mid}} + \frac{\Delta r}{2}) (r_{\text{mid}} \Delta r + \frac{\Delta r^2}{4}) \frac{k_x^2(5k_x^2 - 6k_\omega^2)}{24a^2 k_r^3},$$

$\Delta r$  is the slant range swath width. If  $k_\omega \delta \phi$  is sufficiently small, a simpler separation is simply to fix all range dependence of  $\phi$  at mid-swath  $r_{\text{mid}}$ :

$$Q_{\text{mid}}\left(\frac{k_x}{k_\omega}\right) = \frac{1}{r_{\text{mid}}} \phi\left(\frac{k_x}{k_\omega}, r_{\text{mid}}\right), \quad R_{\text{mid}}(r) = r,$$

which is the method proposed here. As will be seen below, it produces smaller errors than Eq.[8]. The focusing algorithm then becomes similar to Eq.[5] :

$$\bar{S}(k_x, r) = \int dk_\omega \bar{D}(k_x, k_\omega) e^{i k_r r}, \quad (9)$$

$$k_r = k_\omega Q\left(\frac{k_x}{k_\omega}\right).$$

Equation [9] shows that an  $\omega k$  Stolt interpolation, requiring the inversion of the  $k_r(k_x, k_\omega)$  map into a  $k_\omega(k_x, k_r)$  map, focuses the data. The analytic derivative

$$\frac{\partial k_r}{\partial k_\omega} = Q\left(\frac{k_x}{k_\omega}\right) + \frac{k_x}{k_\omega r} \tilde{x}\left(\frac{k_x}{k_\omega}, r\right)$$

is useful in computing the inverse map  $k_\omega(k_x, k_r)$  for  $|k_x/k_\omega| < 1$  and  $|k_r/k_\omega| < 1$  using the Newton-Raphson method, for example.

Equations [5] and [9] need to be rewritten for basebanded quantities to be useful for SAR processing. To do so, range offsets and down-conversion frequencies are introduced. The notation  $X = X_0 + \delta X$  is used for all offsets:

$$\bar{S}(k_x, k_r) = \bar{D}[k_x, k_\omega(k_x, k_r)],$$

$$D(x, \tau) = D^{k_\omega 0}(x, \delta \tau) e^{i k_\omega 0 \tau}, \quad \tau = \tau_0 + \delta \tau, \quad k_\omega = k_\omega 0 + \delta k_\omega,$$

$$\overline{D^{k_\omega 0}}(k_x, \delta k_\omega) e^{-i \delta k_\omega \tau_0} = \bar{D}(k_x, k_\omega),$$

$$S(x, r) = S^{k_r 0}(x, \delta \tau) e^{i k_r 0 r}, \quad r = r_0 + \delta r, \quad k_r = k_r 0 + \delta k_r,$$

$$\overline{S^{k_r 0}}(k_x, \delta k_r) e^{-i \delta k_r r_0} = \bar{S}(k_x, k_r),$$

$$\overline{S^{k_r 0}}(k_x, \delta k_r) = e^{i \delta k_r r_0} e^{-i \delta k_r \tau_0} \overline{D^{k_r 0}}[k_x, \delta k_\omega(k_x, \delta k_r)],$$

where  $k_\omega(k_x, k_r) = k_\omega 0 + \delta k_\omega(k_x, \delta k_r)$  is implied. As in the rectilinear path case, focusing is a 2D phase shift and a 1D  $\omega - k$  interpolation in the wavenumber domain.

The  $\omega k$  processor may also be applied to squinted data [9][2]. A squinted reference system is introduced for the

image domain: these new coordinates  $(r_\psi, x_\psi)$  and their Fourier conjugates are obtained from the orthogonal  $(r, x)$  system through linear transformations:

$$\begin{cases} r = r_\psi \sin \psi, \\ x = x_\psi + r_\psi \cos \psi, \end{cases} \quad \begin{cases} k_{r_\psi} = k_x \sin \psi + k_r \cos \psi, \\ k_{x_\psi} = k_x. \end{cases}$$

Equation [9] can then be adapted to squinted data pro-

cessing using  $\bar{\bar{S}}_\psi(k_{x_\psi}, k_{r_\psi}) = \bar{\bar{S}}(k_x, k_r)$ :

$$\bar{\bar{S}}_\psi(k_{x_\psi}, k_{r_\psi}) = \bar{\bar{D}}\left[k_{x_\psi}, k_\omega(k_{x_\psi}, \frac{k_{r_\psi} - k_{x_\psi} \sin \psi}{\cos \psi})\right].$$

The rotated imaging coordinates  $(r_\psi, x_\psi)$ , however, do not have a straightforward geometrical interpretation due to the curved reference path, as discussed in [8].

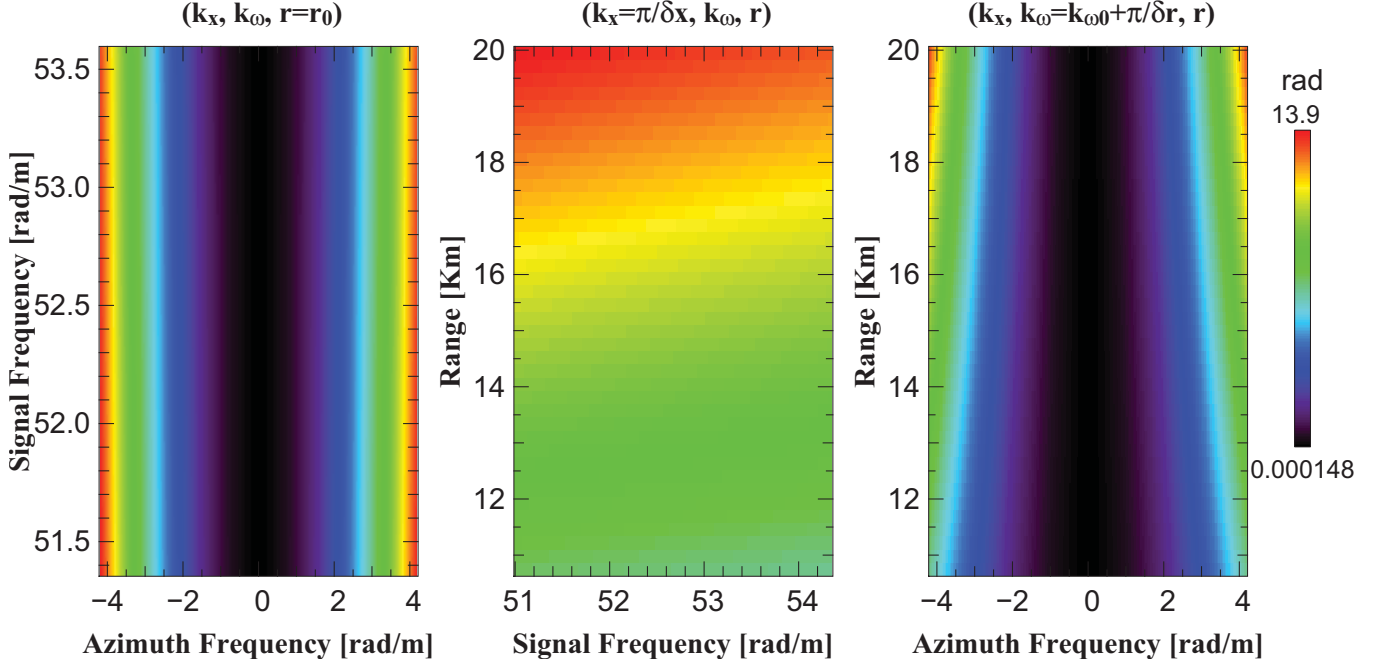


Figure 2. Phase error induced by the antenna track curvature for SAR parameters in Table [1].

## V. APPLICABILITY TO L-BAND AIRBORNE SAR

To evaluate the usefulness of the proposed approach we consider the case of an L-band, airborne SAR dedicated to polarimetric and interferometric applications. The system is similar to the UAVSAR instrument operated by JPL, see Table [1]. The phases error induced by the orbit curvature in this case is shown in Figure [2]. The first panel displays the phase difference  $\Delta k_\omega \phi(k_x/k_\omega, r)$  between the

$h = 10\text{Km}$	platform height, $\theta_{el} = 50^\circ$ ,
$a = 6.4 \cdot 10^6\text{m}$	local earth radius,
$\psi = 15^\circ$	squint angle,
$\nu_0 = 1.26 \cdot 10^6\text{Hz}$	center frequency, $k_{\omega 0} = 4\pi\nu_0/c$ ,
$L_{az} = 1.6\text{m}$	antenna length in azimuth,
$L_{el} = 0.5\text{m}$	antenna length in elevation,
$\Delta\nu = 80\text{MHz}$	radar bandwidth,
$\delta r = 1.66\text{m}$	range resolution,
$\delta x = 0.67\text{m}$	azimuth resolution,
$\Delta r = 10\text{Km}$	$ r - r_{mid} $ : slant range to mid-swath,

Table 1. SAR parameter table.

phase  $k_\omega \phi$  computed in the linear and curved cases, and its main contribution is from the first order term in  $h/a$  in Eq.[7]. The middle panel shows the range dependence at the edge of the Doppler band, and the right-hand panel at the center frequency  $k_{\omega 0}$ . The magnitude of the phase error is 14 radians at maximum, which shows that the track curvature cannot be ignored.

Comparing the exact SP in the curved case to the power series up to  $h^2/a^2$ , the maximal phase error is  $0.01^\circ$ . The second order term  $\phi^{(2)}$  has a non-separable contribution (last term in Eq.[6]), and if that term is ignored the maximal phase error is  $2.5^\circ$ . If the non-separable term is fixed in range at mid-swath  $r_{mid}$ , as in Eq.[8] the maximal phase error is  $1^\circ$ . Finally the proposed method of Eq.[8], has phase errors of  $0.4^\circ$ . A simulated raw SAR data set using parameters found in Table [1] and processed using the mid-swath range separation of Eq.[8] produces a focused image with a structure shown in Figure [3].

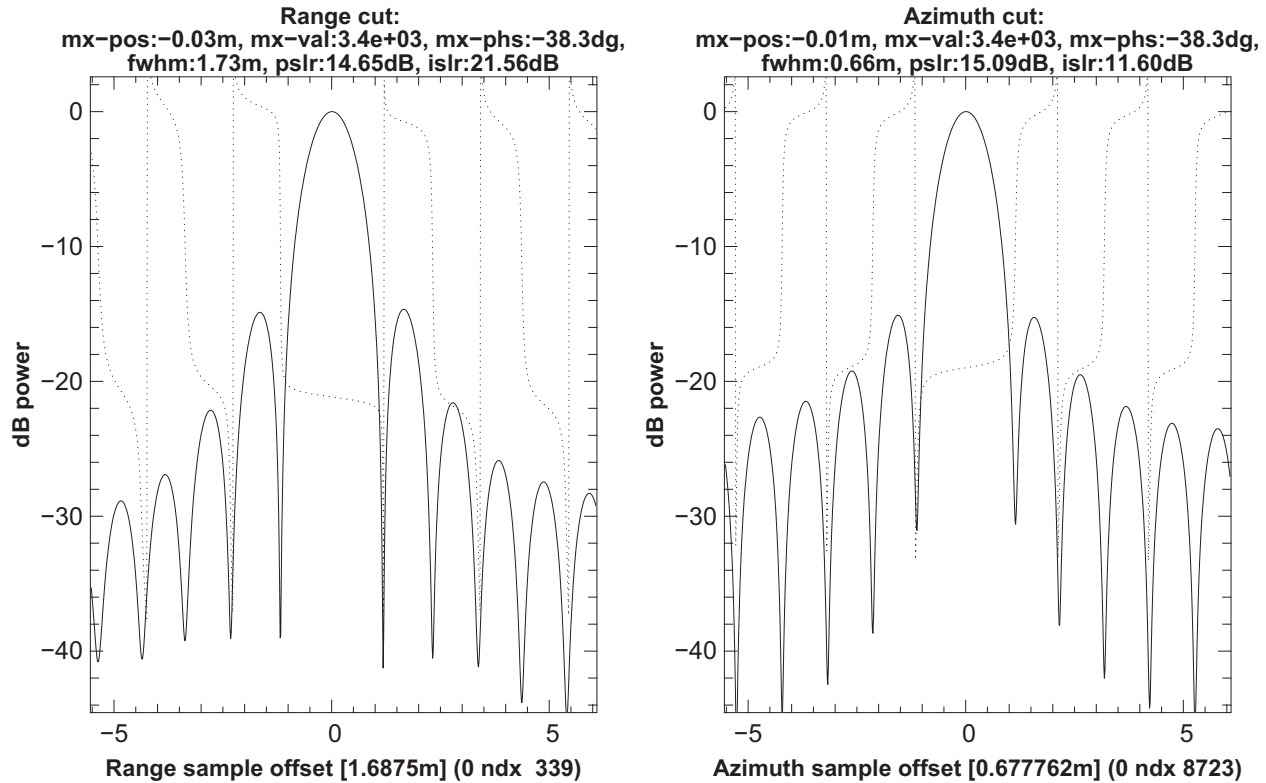


**Figure 3.** Range and azimuth cut of a point target focused using Eq.[8] and simulated using parameters in Table [1]. FWHM is the full width at half maximum in meters, PSRLR is the peak sidelobe to mainlobe power ratio in dB, ISLR is the ratio of the integrated main lobe to sidelobe power in dB, MX-POS is the predicted minus observed image peak position in meters, MX-VAL and MX-PHS are the power and phases at peak amplitude.

## VI. CONCLUSIONS

The applicability of wave domain focusing algorithms may be extended to data acquired on a curved path by using a spherical image reference frame and a modified Stolt map. The optimal  $\omega k$  map is derivable from the phase history at mid-swath. The magnitude of the focusing phase error is of order  $(r^3/a^2)$ . The extended algorithm is compatible with squinted data collected either from an airborne or spaceborne platform.

The research described in this paper was carried out by the Jet Propulsion Laboratory, California Institute of Technology, under contract with the National Aeronautics and Space Administration.

## BIBLIOGRAPHY

- [1] Richard Bamler. A Comparison of Range-Doppler and Wavenumber Domain SAR Focusing Algorithms. *IEEE Transactions on Geoscience and Remote Sensing*, 30(4):706–713, July 1992.
- [2] P. Berens. Extended range migration algorithm for squinted spotlight sar. In *IGARSS 2003, International Geoscience and Remote Sensing Symposium*, volume 6, pages 4053–4055, 2003.
- [3] Ciro Cafforio, Claudio Prati, and Fabio Rocca. SAR Data Focusing Using Seismic Migration Techniques. *IEEE Transactions on Aerospace and Electronic Systems*, 27(2):194–207, March 1991.
- [4] Walter G. Carrara, Ron S. Goodman, and Ronald M. Majewski. *Spotlight Synthetic Aperture Radar: Signal Processing Algorithms*. Artech House Inc., 1995.
- [5] Ian G. Cumming and Frank H. Wong. *Digital Processing of Synthetic Aperture Radar Data: Algorithms and Implementation*. Artech House Inc., Boston, London, 2005.
- [6] Davide D’Aria and Andrea Monti Guarnieri. High-Resolution Spaceborne SAR Focusing by SVD-Stolt. *IEEE Geoscience and Remote Sensing Letters*, 4(4):639–643, Octobre 2007.
- [7] Stewart A. Levin and Fabio Rocca. Dip moveout and stolt migration using the singular value decomposition. *Stanford Exploration Project SEP-56*, pages 191–202, 1987.
- [8] Johan Jacob Mohr and Søren Nørvang Madsen. The Impact of Curved Satellite Tracks on SAR Focusing. In *IGARSS 2000, International Geoscience and Remote Sensing Symposium*, pages 87–89, 2000.
- [9] A. Monti-Guarnieri, C. Prati, and F. Rocca. Sar focusing in non-standard geometries: A generalized approach. In *IGARSS 1992, International Geoscience and Remote Sensing Symposium*, pages 369–371, 1992.
- [10] Claudio Prati, Fabio Rocca, Andrea Monti-Guarnieri, and Elvio Damonti. Seismic Migration For Sar Focusing: Interferometrical Applications. *IEEE Transactions on Geoscience and Remote Sensing*, 28(4):627–640, July 1990.
- [11] Fabio Rocca. Synthetic Aperture Radar: a New Application for Wave Equation Techniques. *Stanford Exploration Project SEP-56*, pages 167–189, 1987.
- [12] R. H. Stolt. Migration by Fourier Transform. *Geophysics*, 43(1):23–48, Feb 1978.